(Preprint) AAS 17-310

CORRELATION OF OBSERVATIONS AND ORBIT RECOVERY CONSIDERING MANEUVERS

J.A. Siminski*, H. Fiedler†, and T. Flohrer‡

Optical tracklets collected after or during a maneuver phase cannot be directly associated to any cataloged object. The observations do not provide enough information for an independent orbit determination. Thus, the new orbit remains uncertain before collecting any additional measurements. Two methods for the correlation and orbit recovery are presented. First, the solution space after the maneuver is bounded using an admissible region. Second, the historic maneuver data of each object is characterized to compute the association likelihood and predict the most likely state after a maneuver. The performance of the presented approaches is demonstrated using data of EUMETSAT satellites.

INTRODUCTION

Satellites typically maintain or establish their operational orbit by performing impulsive or continuous thrust maneuvers. When cataloging resident space objects, these rapid or slow orbital changes complicate a successful correlation. That is, measurements collected after a maneuver cannot be directly associated to any cataloged object. Short optical observations arcs, so-called tracklets, do not provide enough information for an independent orbit determination. Hence, multiple of these arcs are required to recover the orbit after the maneuver. Before collecting these additional measurements, the new orbit remains uncertain and hence cannot be used for operational support, e.g. to detect conjunction events. These difficulties motivate a more advanced correlation and recovery method using all available information.

Before starting the orbit recovery, the measurements must be associated to the cataloged objects. Otherwise the catalog size would artificially increase without actually adding any new objects to the domain. Holzinger et al.[1] and Singh et al.[2] propose to use a control effort distance metric to rank different possible object associations, i.e. the object which realizes the measurement with the least fuel consumption is the most likely originator. The fuel consumption is commonly described with a ΔV-budget. As suggested by Singh et al.,[2] a ΔV - threshold can be defined to associate measurements to objects, which could realize the observation with a feasible or common amount of fuel. The orbital solution which requires the least amount of ΔV is then considered the most likely state after the maneuver.[1] Even though operators will likely use efficient maneuvers, their optimal maneuver does not need to coincide with the minimum ΔV solution realizing the new measurement arc as a different objective function is optimized.

*Space Debris Engineer, IMS Space Consultancy at ESA/ESOC Space Debris Office, Robert-Bosch-Str. 5, 64293 Darmstadt, Germany

†Head of Space Situational Awareness group, DLR/GSOC, Münchner Str. 20, 82234 Weßling, Germany

‡Space Debris Analyst, ESA/ESOC Space Debris Office, Co-Lead Space Surveillance and Tracking Segment, Space Situational Awareness Programme.

This work introduces two additions after the first loose association step. First, the current approach to recover the orbit using the minimum energy trajectory[1] is extended to account for unknown maneuver strategies. A ΔV-admissible region is defined, which bounds the feasible solution space after the maneuver. All solutions within this region then represent candidate states of the catalog object. In the second proposed approach, historic maneuver data of each object is analyzed to estimate the association likelihood and predict the most likely state. The maneuver history can be obtained from satellite operators or estimated from cataloged states. An example of the latter estimation is given by Lemmens and Krag[3] who detect maneuvers from the publicly available Two-line element catalog (*space-track.org*).

Both approaches are illustrated by showing the observation correlation and recovery of the most likely orbital state. They are assessed with reference ephemerides and maneuvers reported by EUMETSAT for two of their active satellites. In the last section, the accuracy of the recovered states of both methods is compared.

MINIMUM ENERGY SOLUTION

As proposed by Holzinger et al.[1] and Singh et al.,[2] the orbit of a satellite after a maneuver can be recovered assuming that the operators performed the maneuvers in an optimal way, i.e. using the least amount of fuel. Let $\boldsymbol{y}_b$ at t_b be the known orbital state of a cataloged object right before the maneuver and $\boldsymbol{y}_a$ at t_a the unknown after it. The trajectory connecting the two states is described with the ordinary differential equation

$$\dot{\boldsymbol{y}} = \boldsymbol{f}(\boldsymbol{y}(t), \boldsymbol{u}(t), t)\,, \tag{1}$$

where $\boldsymbol{u}$ is the thrust control and is included as an additional acceleration in the equations of motion. The fuel consumption ΔV_T is commonly bounded using the quadratic loss[1]

$$\Delta V_T \leq \Delta V(\boldsymbol{y}_b, \boldsymbol{y}_a) = \sqrt{2(t_a - t_b)P} \tag{2}$$

where

$$P = \min\left\{\frac{1}{2}\int_{t_b}^{t_a} \boldsymbol{u}(t)^\mathsf{T}\boldsymbol{u}(t)\,\mathrm{d}t\right\} \tag{3}$$

describes the minimum energy solution of a trajectory connecting $\boldsymbol{y}_b$ and $\boldsymbol{y}_a$. It is minimized with optimal control problem solvers (here the one by Houska et al.[4] is used) and is commonly easier to find than the direct solution giving the smallest possible ΔV_T.

A new optical tracklet $\boldsymbol{z} = (\boldsymbol{s}, \dot{\boldsymbol{s}})$ at t_a constrains the satellite state in four degrees of freedom, i.e. two angles and their rates. Instead of using angles, the information of the tracklet is represented here with the line-of-sight $\boldsymbol{s}$ and its time-derivative $\dot{\boldsymbol{s}}$. When augmenting the observation $\boldsymbol{z}$ with the range and range-rate $\boldsymbol{x} = (\rho, \dot{\rho})^\mathsf{T}$, a state hypothesis at t_a is given

$$\tilde{\boldsymbol{y}}_a(\boldsymbol{x}) = \begin{pmatrix} \boldsymbol{R} + \rho\boldsymbol{s} \\ \dot{\boldsymbol{R}} + \dot{\rho}\boldsymbol{s} + \rho\dot{\boldsymbol{s}} \end{pmatrix}, \tag{4}$$

where $\boldsymbol{R}$ and $\dot{\boldsymbol{R}}$ denote the station position and velocity. The most likely state assuming the minimum energy trajectory is accordingly given by

$$\hat{\boldsymbol{x}} = \arg\min_{\boldsymbol{x}} \Delta V(\boldsymbol{y}_b, \tilde{\boldsymbol{y}}_a(\boldsymbol{x}))\,. \tag{5}$$

ΔV-admissible region

The minimum energy solution does not need to coincide with the true state after the maneuver as maneuvers. Operators typically perform maneuvers that guarantee long-term fuel efficiency and safe operations. This objective function does not need to have the same minimum as when finding the solution which best approximates the new measurement arc. In case of further constraints, e.g. limiting the maneuvers to work hours, the assumptions for the minimum energy solution become even less valid. The dataset used for this work does not contain maneuver planning with work hour constraints.

Instead of recovering the orbit with one single hypothesis, a region of possible solutions represents all states after the maneuver. The admissible region concept is applied to the case of maneuver orbit reconstruction. Milani et al.[5] introduce the admissible region concept to restrict the solution domain $\mathcal{C}$ of possible asteroid orbits to a small tractable domain. Tommei et al.[6] require the orbits of debris objects to be stable around Earth.

Defining the state hypothesis with Equation (4) and inserting it into (2), the ΔV-admissible region is bounded with

$$\mathcal{C}(\boldsymbol{z}) = \{\boldsymbol{x} : \Delta V(\boldsymbol{y}_b, \tilde{\boldsymbol{y}}_a(\boldsymbol{x})) \leq \Delta V_{\text{max}} \,. \tag{6}$$

The principle of the admissible region generation in case of orbital maneuvers is illustrated in Figure 1. It shows the cataloged state $\boldsymbol{y}_b$, the new observation $\boldsymbol{z}$, and three possible states after the maneuver epoch: the state considering no maneuver (leading to no association) and the true solution $\boldsymbol{y}_a$ as well as the minimum energy solution $\boldsymbol{y}_a^*$ are shown inside the admissible region. The solution $\boldsymbol{y}_a^*$ which minimizes the ΔV can be assumed as the most likely candidate and serves as an initial estimate for the post-maneuver state.

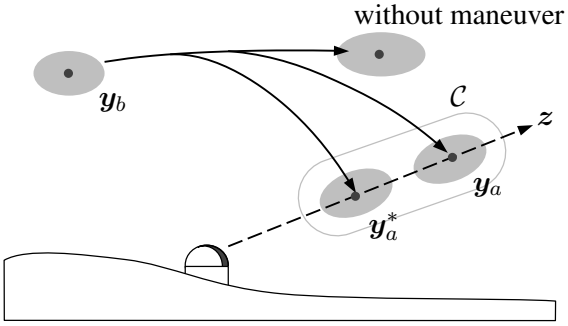

Figure 1: Admissible region $\mathcal{C}$ for new observation $\boldsymbol{z}$ given the pre-maneuver state $\boldsymbol{y}_b$.

Figure 2 shows the required ΔV depending on $\boldsymbol{x}$ for the geostationary satellite Meteosat-9. A series of observations is simulated using the reference states and the line-of-sight and its time-derivative is derived thereof. The reference ephemerides before ($\boldsymbol{y}_b$) and after the maneuver ($\boldsymbol{y}_a$) are obtained from the weekly orbits published by EUMETSAT. The white lines illustrate levels of constant ΔV and are potential boundaries for the admissible region. A boundary can be defined by allowing certain maneuver types and could also depend on the longitude of the satellite (considering the different ΔV requirements.[7]). The minimum of the evaluated function (estimate of the post-maneuver state $\boldsymbol{y}_a^*$) is depicted with a cross ($\times$) in the figure. The difference between reference and the estimated range $\Delta\rho$ is around a few kilometers and for the estimated range-rate $\Delta\dot{\rho}$ in the m/s range.

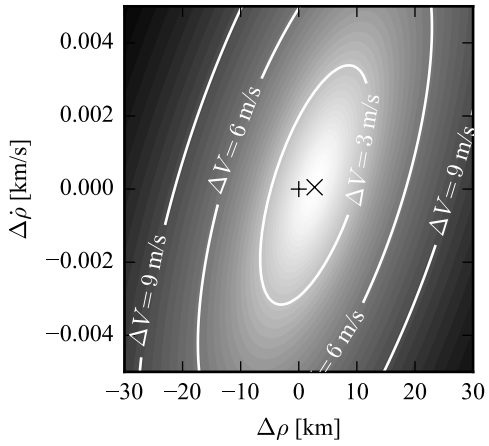

Figure 2: ΔV requirement depending on $\boldsymbol{x}$ (relative to the reference solution ($+$) in the center). The solid white lines bound admissible regions which allow a certain ΔV_{max}. The minimum ΔV solution $\boldsymbol{y}_a^*$ is shown with the $\times$.

In order to fully reconstruct the orbit after the maneuver, the solution space must be sampled with hypotheses where each one is then tested against incoming new observations. The surviving hypothesis will then update the cataloged state (cf. Gaussian-mixture filtering[8]). Similarly, the optimization approach[9] can be used for the association of new measurements allowing only combinations with a feasible solution within the ΔV-restricted admissible region.

ESTIMATION BASED ON HISTORIC DATA

A new alternative approach is presented which uses historic data of the satellite. Satellites can perform multiple maneuvers between two observation epochs. Hence, the exact maneuver epoch and ΔV is unknown and can not be estimated from sparse observations, e.g. one new tracklet every day or every few days. However, the cataloged post and pre-maneuver states can be determined from an orbit determination process. The information from the past maneuver states is used to characterize the orbital change. The information is first transformed into a state, called *feature vector*, which can be used for the prediction.

Let $\boldsymbol{y}_b^i$ at t_b^i be all the past orbital states right before the maneuvers and $\boldsymbol{y}_a^i$ at t_a^i directly after the maneuvers ($i = 1, \ldots, n$, where n is the number of past maneuvers). The orbital change is often better described in terms of mean orbital elements. Rapid short-term variations in the orbit could be erroneously identified as a maneuver even though they are effectively caused by the natural dynamics. Similarly, operators use mean element formulations for the maneuver planning.[10] Thus, the state vectors $\boldsymbol{y}_b^i$ and $\boldsymbol{y}_a^i$ are transformed to mean elements using the formulation by Kamel[11] which was specifically developed for satellites on geostationary orbits.

A maneuver can be described with various variables:

1. A change in orbital elements is dependent on the current state $\boldsymbol{y}_b^i$, e.g. whenever a geostationary satellite reaches its box boundaries, it will most likely perform an East-West maneuver.

2. Maneuvers are likely to be performed after similar time-intervals Δt^i (due to similar dynamics

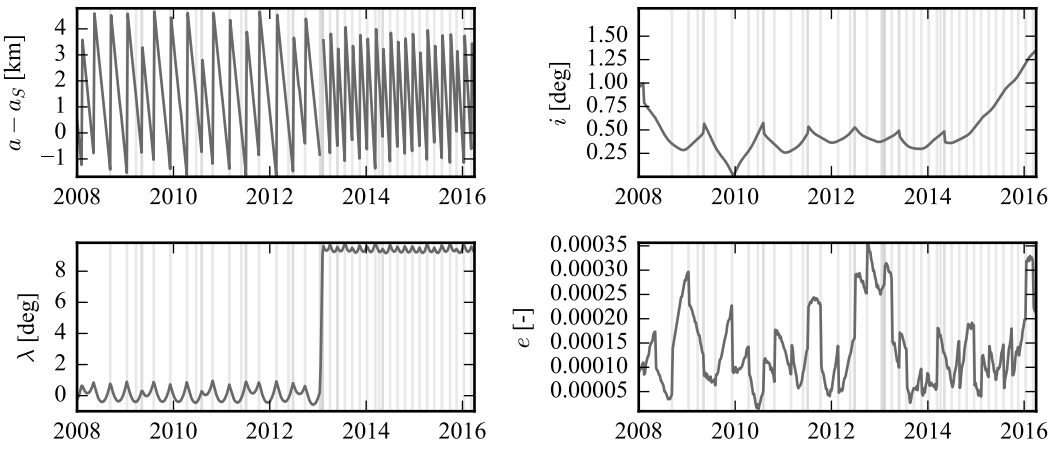

Figure 3: Time series of mean orbital elements for Meteosat-9: semi-major axis a w.r.t. to the synchronous a_S, inclination i, longitude λ, eccentricity e.

causing a deviation from the nominal orbit and due to human operator practice).

3. Station-keeping maneuvers typically repeatedly require the same amount of fuel described with ΔV^i. For instance, East-West maneuvers, when performed regularly, need a certain amount of fuel depending on the sub-satellite longitude.[7] Inclination control requires a different amount of fuel and depends on the epoch (due to luni-solar perturbations).

Figure 3 shows the time series of selected mean orbital elements for Meteosat-9, obtained from the reference ephemerides which are reported weekly by EUMETSAT. The light-grey lines illustrate the maneuver epochs as reported by EUMETSAT by email.[12] The maneuver epochs coincide with changes in the above listed variables.

The time series will look different when satellites use a continuous thrust over long time periods to maintain their orbital position. Describing these strategies with instantaneous changes in the above defined variables would not well represent the maneuvers. However, other variables can be found to group the maneuver types, e.g. the rate of change of orbital elements over time. However, the available dataset by EUMETSAT contains only satellites with instantaneous orbital changes. Therefore, this analysis focuses on these maneuver strategies.

The repeating patterns of maneuvers as observed in Figure 3 allows to estimate a probability density function of future states based on the historic data of the object. Starting from the latest orbital state in the catalog $\boldsymbol{y}_b^{n+1}$ and assuming that a maneuver has been performed, some orbital states at the next observation epoch t_a^{n+1} are more likely than others. Shabarekh et al.[13] uses machine learning algorithms (or pattern learning) to predict the maneuver likelihood in the future.

This work describes the relationship between the variables using the so-called kernel density estimation.[14] The characteristics of maneuvers are described with the feature vector, which contains some of the pre-maneuver mean elements $\boldsymbol{e}_b^i$ (consisting of semi-major axis a, mean longitude λ, inclination i, and eccentricity e), the past maneuver elements $\boldsymbol{e}_a^i$, their difference $\Delta\boldsymbol{e}^i$ and the time difference w.r.t. to the last maneuver. Instead of using the full set of orbital elements, a subset is used which is sufficient to describe geostationary orbits. The final vector used in this work to

describe a maneuver is

$$\boldsymbol{c}^i = (\boldsymbol{e}_b^i, \boldsymbol{e}_a^i, \Delta\boldsymbol{e}^i, \Delta t^i)\,. \tag{7}$$

The probability density for any new state after the maneuver $\boldsymbol{y}_a^{n+1}$ is then expressed in terms of the historic data $\boldsymbol{c}^i$ with the following equation

$$f(\boldsymbol{y}_a^{n+1}) = \sum_i^n \boldsymbol{k}_h(\boldsymbol{c}^{n+1}(\boldsymbol{y}_a^{n+1}) - \boldsymbol{c}^i)\,, \tag{8}$$

where $\boldsymbol{k}_h$ is a smoothing kernel with bandwidth h and $\boldsymbol{c}^{n+1} = (\boldsymbol{e}_b^{n+1}, \boldsymbol{e}_a^{n+1}, \Delta\boldsymbol{e}^{n+1}, \Delta t^{n+1})$. The latter feature vector is obtained by transforming the state into the respective mean elements and computing the time difference to the last observed maneuver. Various choices for smoothing kernels are discussed in the literature along with strategies how to select the bandwidth.[15] A Gaussian kernel is selected with Silverman's rule of thumb for the bandwidth selection.[15] Additionally a *forgetting factor* ϕ is introduced which reduces the impact of old maneuvers on the density function (effectively down-weights the respective older samples). Each kernel is multiplied with a weight $w^i = \phi^{t^{n+1}-t^i}$ depending on how old the maneuver of the kernel is. A typical choice for ϕ is 0.99. A smaller value will decrease the weight for older samples. This weighting becomes important if a maneuver strategy is changed (e.g. when placing a satellite from its parking orbit into the operational slot).

Figure 4 shows the probability density function for different variable combinations. Darker area means more samples in the past and thus more likely. As also visible in the inclination time series, two types of maneuvers exist: one group which performs no inclination change (accumulation of many samples on the right-hand side plot) and a much smaller one which does (*North-South* station keeping). A semi-major axis change is likely once the longitudes around $9.5^\circ - 9.7^\circ$ are reached. However, the satellite was relocated from around 0°. The old samples are weighted less than newer ones and consequently do not contribute much to the density function. Lastly, the left-hand side plot shows that the maneuvers after relocation are typically performed once every 60 days for this satellite.

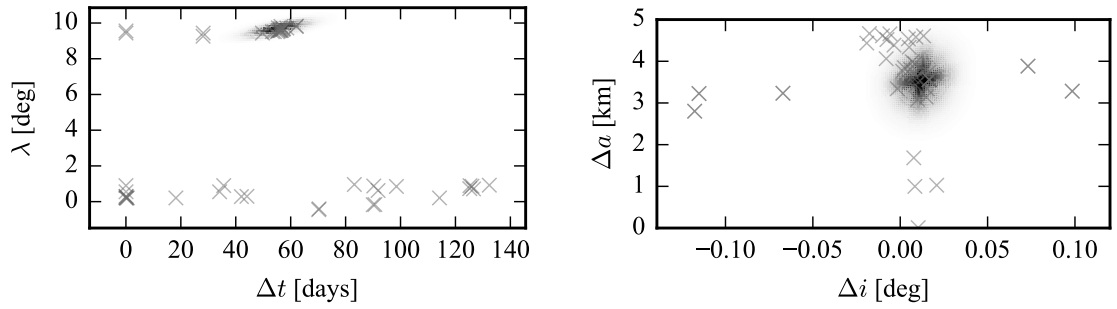

Figure 4: Probability density of orbital changes, pre and post-maneuver states and time since the last maneuver.

Association of new observations and recovery

The cataloged object state before the maneuver is again denoted with $\boldsymbol{y}_b$ at t_b for notational simplicity (dropping the superscript index). When a new measurement $\boldsymbol{z}$ at t_a is tested against all catalog states leading to no successful associations, a maneuver must have been performed or a new object was placed in orbit (neglecting losses due to unpredictable natural dynamics). Again, the four-dimensional observation $\boldsymbol{z}$ reduces the orbital solution space to a two-dimensional plane, which can be parametrized with the range and range-rate $\boldsymbol{x} = (\rho, \dot{\rho})$. The plane cuts through the density function in (8) resulting in a two-dimensional probability density function. The procedure is illustrated in Figure 5. Besides showing the density on the intersecting plane, the traditional admissible region[6] and the ΔV-admissible region are illustrated. The density function for the post-maneuver state is then computed from inserting Equation (4) into (8)

$$f(\boldsymbol{x}) = \sum_{i}^{n} \boldsymbol{k}_h(\boldsymbol{c}(\boldsymbol{x}) - \boldsymbol{c}^i)\,. \tag{9}$$

The approximate Δt is computed from t_a and the last estimated maneuver epoch. All other orbital elements required for $\boldsymbol{c}$ are computed from $\boldsymbol{x}$ and the new observation vector $\boldsymbol{z}$.

The most-likely orbital solution using the density function is then given by

$$\hat{\boldsymbol{x}} = \arg\max_{\boldsymbol{x}\in\mathcal{C}} f(\boldsymbol{x}) \tag{10}$$

and consequently if multiple catalog states are tested with one new measurement, the one with the largest probability is the most promising candidate for the association.

Figure 6 shows the density for the same simulated observation of Meteosat-9 as used in Figure 2. The maximum of the probability w.r.t. to the reference solution in the center is again indicated with the white cross ($\times$). The error in range and range-rate for this example is around 100 m and 0.1 m/s. This result comes therefore closer to the reference state when compared to the minimum energy solution. The density is computed from 50 pre- and post-maneuver states of Meteosat-9 from 2008 to 2016. Meteosat performed one relocation maneuver, seven North-South station keeping maneuvers and otherwise East-West maneuvers in this time period.

If multiple candidate objects can be associated with a similar probability, each one can be loosely associated using the probability as an association weight. As the density function in (8) is not

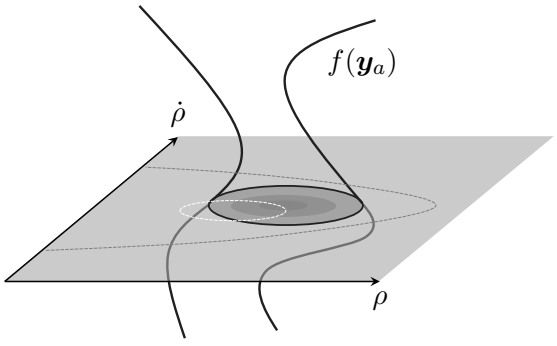

Figure 5: Illustration of the density function intersection with the plane of orbital solutions. The gray dashed line surrounds the admissible region as defined by e.g. energy constraints,[5].[6] The white dashed line surrounds the ΔV-admissible region $\mathcal{C}$ as defined in equation (6).

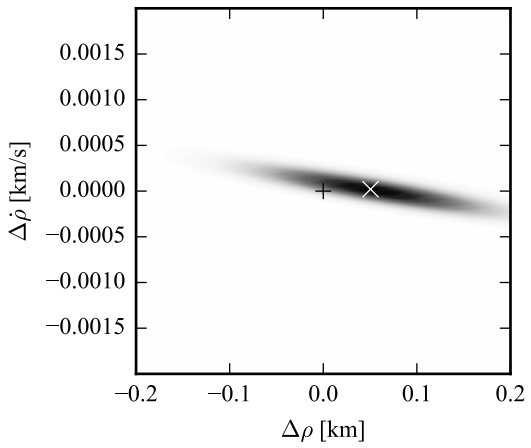

Figure 6: Probability density function of orbital state given a new measurement. Range and range-rate are centered around the reference solution (+). The white cross (×) depicts the maximum of the density function.

necessarily unimodal, the corresponding density function in range and range rate can be multimodal as well and thus allows for multiple feasible solutions. The whole ΔV-admissible region can be sampled with hypotheses and every hypothesis with negligible probability is discarded.

COMPARISON

Both presented approaches are compared in the following. As both are able to correlate the simulated measurements to the cataloged objects for the tested dataset, the main goal of this section is to assess the accuracy of the resulting post-maneuver state. The last 10 epochs are used to select the states before and after the maneuvers from the weekly orbits. The kernel density estimation considers only states in the past, e.g. 40 for the first tested epoch, 41 for the next and so forth. All observed maneuvers within this sequence are East-West station keeping maneuvers. The density function and the ΔV-function are optimized using the same numerical optimization routine (*optimize.minimize*) from the SciPy library.[16] The synchronous semi-major axis serves to compute an initial starter for the optimization. In case of the kernel density function f, a bad starter can fall into a region with numerically zero probability. Hence, if an iterative optimizer will not find a gradient or better value in the close vicinity of the starter, it will fail to converge. This behavior was only observed when artificially placing starters far away from the solution. However, the density function can be initially sampled on a grid to find the local maxima. From thereon the iterative solvers are capable of finding the most likely solution.

The differences between reference and obtained solutions is shown in Figure 7. It shows the errors in range and range-rate for a set of epochs after a maneuver was performed. The kernel density function estimate predicts the reference state after the maneuver better by one order of magnitude. This performance difference is as expected as all tested maneuver types were observed before. The test is repeated for Meteosat-10, where ephemerides and maneuver epochs are available from 2012 to 2016. Within this time period, the satellite performed in total 15 maneuvers. After an initial relocation, it performed 11 East-West and 1 North-South station keeping maneuvers. The dataset is smaller compared to the first test. Hence, less test epochs (5) from the back of the time

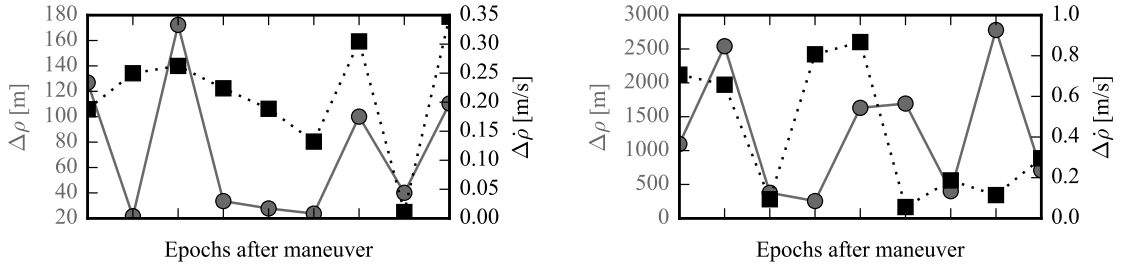

Figure 7: Difference between predicted and estimated post-maneuver states using the historic data (left) and the minimum energy solution (right) for the last 10 maneuver epochs of the Meteosat-9 dataset. The gray circles depict the range differences and the black squares depict the range-rate differences.

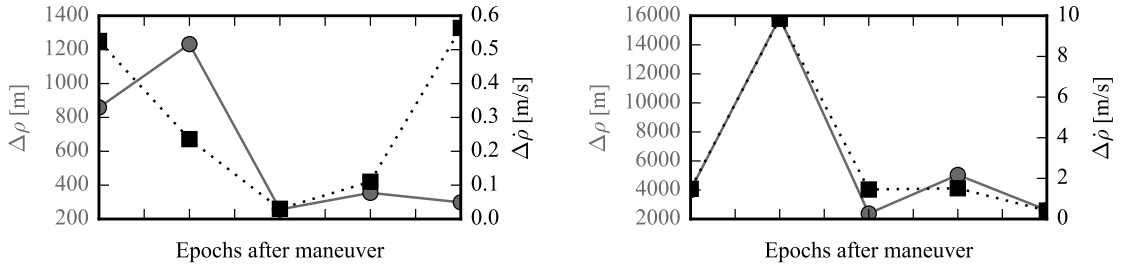

Figure 8: Difference between predicted and estimated post-maneuver states using the historic data (left) and the minimum energy solution (right) for the last 5 maneuver epochs of the Meteosat-10 dataset. The gray circles depict the range differences and the black squares depict the range-rate differences.

series are selected. The results are shown in Figure 8 and are particularly interesting as the first and never learned North-South maneuver appears at the second tested epoch.

Except for the second epoch, the minimum energy solution shows a similar performance as for the previous Meteosat-9 sample. However, the minimum energy trajectory connecting the new observation and the last cataloged state seems to be very different in case of the North-South maneuver. In case of the kernel density estimate, the performance is in general worse than in the Meteosat-9 case but still better than the minimum energy solution. This can be explained by the smaller amount of learning samples. The orbit after the second maneuver (not yet learned from the data) is still recovered with an error of about 1 km in range. This indicates that the changed inclination is largely determined from the new observed tracklet and does not require many learning samples.

Run-time comparison

The optimization requires around 3 seconds for the 10 correlation tests of the Meteosat-9 example using the kernel density estimate and around 3 minutes for the minimum energy solution. The tests were performed on a 2.4 GHz Intel Core i5 laptop and both tests are written in Python. The optimal control problem within the minimum energy solution computation is solved using a C++ optimal control solver.[4] This expensive subproblem makes the minimum energy solution more

computationally expensive. The solver is called with a wrapper from Python. The formulation of the optimization problem could be altered to improve run-time performance. The kernel density estimation code is not optimized for large data sets (e.g. using K-D trees for evaluation), i.e. every kernel must be evaluated to find the probability of a certain solution. This is sufficiently fast for the relatively small number of maneuvers of geostationary satellites, but could be improved in case of lower objects. The performance of the methods can be also further improved by using a compiled programming language such as C++.

CONCLUSION AND OUTLOOK

Two different methods are presented to correlate new measurements to already cataloged maneuvering objects and recover their orbits after the maneuver. The first is the minimum energy solution, adapted from Holzinger et al.,[1] the second is newly developed and includes historic data into the estimation process. The performance of both methods is very promising as the simulated measurements are successfully correlated. The accuracy of the kernel density method appears to be better. However, this is only true as long as the maneuvers are predictable. The minimum energy solution and the ΔV-admissible region sample can always serve as a fall-back option when no historic information is available.

In the framework of space object behavior understanding, objects are classified into groups e.g. by the different operational maneuver strategies.[17] The catalog data (e.g. orbital states, measurements) can be merged with additionally information sources (e.g. operator data, news articles, etc.) to describe the expected spacecrafts motion. If such a database is available, individual methods to predict the post-maneuver state depending on the satellite class could be developed. The here used kernel density estimation is a simple and robust way of describing the orbital change. However, more advanced prediction methods and more available object information can improve the performance. The principle idea of merging the new observations with the probable state density remains the same and could be also applied when using another density prediction tool.

This work uses simulated observation for the proof of concept. Future work will investigate the success of the method with real observations. Additionally the quality of the resulting orbits will be assessed further, e.g. if it suffices to successfully correlate the determined state with following observations.

REFERENCES

[1] M. J. Holzinger, D. J. Scheeres, and K. T. Alfriend, "Object correlation, maneuver detection, and characterization using control distance metrics," *Journal of Guidance, Control, and Dynamics*, Vol. 35, 2012, pp. 1312–1325.

[2] N. Singh, J. T. Horwood, and A. B. Poore, "Space object maneuver detection via a joint optimal control and multiple hypothesis tracking approach," *Proceedings of the 22nd AAS/AIAA Space Flight Mechanics Meeting*, Vol. 143, 2012.

[3] S. Lemmens and H. Krag, "Two-line-elements-based maneuver detection methods for satellites in low earth orbit," *Journal of Guidance, Control, and Dynamics*, Vol. 37, 2014, pp. 860–868.

[4] B. Houska, H. J. Ferreau, and M. Diehl, "ACADO toolkit: An open-source framework for automatic control and dynamic optimization," *Optimal Control Applications and Methods*, Vol. 32, No. 3, 2011, pp. 298–312.

[5] A. Milani, G. F. Gronchi, M. d. Vitturi, and Z. Knežević, "Orbit determination with very short arcs. I admissible regions," *Celestial Mechanics and Dynamical Astronomy*, Vol. 90, No. 1-2, 2004, pp. 57–85.

[6] G. Tommei, A. Milani, and A. Rossi, "Orbit determination of space debris: admissible regions," *Celestial Mechanics and Dynamical Astronomy*, Vol. 97, No. 4, 2007, pp. 289–304.

[7] E. M. Soop, *Handbook of geostationary orbits*, Vol. 3. Springer Science & Business Media, 1994.

[8] K. DeMars and M. Jah, "Probabilistic initial orbit determination using gaussian mixture models," *Journal of Guidance, Control, and Dynamics*, Vol. 36, 2013, pp. 1324–1335.

[9] J. Siminski, O. Montenbruck, H. Fiedler, and T. Schildknecht, "Short-arc tracklet association for geostationary objects," *Advances in Space Research*, Vol. 53, No. 8, 2014, pp. 1184–1194.

[10] H. Schaub and K. T. Alfriend, "Impulsive feedback control to establish specific mean orbit elements of spacecraft formations," *Journal of Guidance, Control, and Dynamics*, Vol. 24, No. 4, 2001, pp. 739–745.

[11] Kamel, A. A., "Geosynchronous satellite perturbations due to Earth's triaxiality and luni-solar effects," *Journal of Guidance, Control, and Dynamics*, Vol. 5, No. 2, 1982, pp. 189–193.

[12] M. Klinc. personal communication.

[13] C. Shabarekh, J. Kent-Bryant, G. Keselman, and A. Mitidis, "A Novel Method for Satellite Maneuver Prediction," *Advanced Maui Optical and Space Surveillance Technologies Conference*, 2016.

[14] E. Parzen, "On Estimation of a Probability Density Function and Mode," *The Annals of Mathematical Statistics*, Vol. 33, 09 1962, pp. 1065–1076.

[15] B. W. Silverman, *Density estimation for statistics and data analysis*, Vol. 26. CRC press, 1986.

[16] E. Jones, T. Oliphant, P. Peterson, *et al.*, "SciPy: Open source scientific tools for Python," [Online; accessed 2016-12-01].

[17] R. Furfaro, R. Linares, D. Gaylor, M. Jah, and R. Walls, "Resident Space Object Characterization and Behavior Understanding via Machine Learning and Ontology-based Bayesian Networks," *Advanced Maui Optical and Space Surveillance Technologies Conference*, 2016.